

Quadrupole Topological Insulator in Non-Hermitian Thermal Diffusion

Guoqiang Xu^{1#}, Xue Zhou^{2#}, and Cheng-Wei Qiu^{1*}

¹*Department of Electrical and Computer Engineering, National University of Singapore, Kent Ridge 117583, Republic of Singapore*

²*School of Computer Science and Information Engineering, Chongqing Technology and Business University, Chongqing, 400067, China*

[#]These authors contributed equally.

^{*}Correspondence to: chengwei.qiu@nus.edu.sg

Abstract

Higher-order topological insulator (HOTI) has unveiled a new type of band topology with bulk multipole moment, resulting in the nontrivial topology in D -dimensional gapped bulk and simultaneously hosting the quantized invariants for gapless modes on $(D-1)$ -dimensional boundaries. All state-of-the-art strategies for topological heat transport fail to observe such higher-order hierarchical features, since the absence of multipole moments in diffusion fundamentally forbids the corresponding expansion of bulk topology. Here, we report the paradigm of creating bulk quadrupole moments in diffusion, thus enabling the HOTI in non-Hermitian thermal systems. The experiments showcase that both the real- and imaginary-valued bands support the hierarchical hallmarks of bulk, gapped edge, and in-gap corner states, in stark contrast to the higher-order states only observed on real-valued bands in classic wave fields. Our findings open a new chapter of diffusive manipulations and add a new candidate for higher-order topological physics.

Topological states of matter have found explosive developments across various classic wave fields [1-5]. In an adiabatic system, hermiticity lies at the foundation of these emerging topological properties [6, 7], as it ensures the real-valued eigenvalues and the orthogonal eigenstates. When considering open systems, additional interactions with ambient

raise the non-hermiticities. Though these dissipations fail the fundamental bulk-boundary correspondence [8, 9] defined in Hermitian system, a plethora of more exotic properties are empowered, such as parity-time symmetry [10-12], Weyl exceptional ring [13, 14], and skin effects [15, 16]. The newly predicted higher-order topological insulators (HOTI) have further paved an avenue of studying hierarchical features both in Hermitian [17-22] and non-Hermitian [23-26] systems. Featuring a nontrivial quadrupole moment [17], the Benalcazar-Bernevig-Hughes (BBH) model holds the key for realizing a minimal quadrupole topological insulator (QTI) possessing positive and negative couplings [17-19]. Besides, a modified non-Hermitian BBH model indicates that both the on-site non-hermiticities [23] and the hermiticities [24] can derive the quadrupole phase and modulate the higher-order transitions [23-26].

It is recently found that dissipative diffusion is fundamentally governed by skew-Hermitian physics and characterized by a purely imaginary Hamiltonian [27, 28]. Thus it activates the long-ignored topological features in heat transport, such as non-Hermitian topological insulating phases [29] and Weyl exceptional rings [30]. On the other hand, the state-of-the-art methods [27-30] fail to create non-Hermitian thermal HOTIs in both theories and experiments, since the absent bulk quadrupole moment and undefined negative couplings in heat exchanges forbid their exhibitions. Hence, non-Hermitian BBH model seems infeasible in heat transport, and higher-order thermal transitions are still elusive at large.

Here, we create the thermal quadrupole moment with same-strength hot and cold sources, and reveal the non-Hermitian HOTI in thermal diffusion for the very first time. It is essentially realized by enabling effective positive and negative couplings in temperature fields via configuring the heat exchange directions between neighboring sites. In stark contrast to the higher-order features only observed on real-valued bands in classic wave fields, we capture these states on both real- and imaginary-valued bands. We then experimentally demonstrate these higher-order thermal states, and separately observe significant temperature localizations at the bulk, edge, and corner of the fabricated samples. Our work indicates a paradigm for establishing the HOTI in thermal systems and unlocking rich topological phase transitions in heat transport. The findings also suggest exotic physics in more diffusive territories [31-35].

We first consider a discrete grid domain consisting of a convective thermal system with multiple sites as illustrated in Fig. 1a. Each site indicates the carrier of heat transfer process in a finite volume, while the grid lines between neighboring sites describe their thermal couplings via tailored connections. We adopt tunable advections on each site to provide modulated components and create effective resonances in the thermal system, thus further forming an effective unit-structure with four neighboring sites (Fig. 1b). Further periodically configuring such unit-structures, an effective 2D primitive square-lattice with 16 sites can be indicated in the thermal system. The general heat transfer process of each site within one unit-structure can be expressed as

$$\frac{\partial T_{ij}}{\partial t} = \frac{\kappa}{\rho c} \nabla^2 T \pm \omega_{I/II} R(\theta) \nabla T + \sum \beta h \Delta T. \quad (1)$$

In Eq. (1), ρ , c , and κ respectively denote the density, specific heat, and thermal conductivity. $\omega_{I/II}$ represents the amplitude of the resultant angular velocities imposed on each site, while R and θ respectively denote the radial and azimuth components in the x - y plane. h indicates the heat transfer coefficient along x / y directions of the selected site. β is the ratio between the intercell and intracell heat exchanges, and its value is 1 when the media and structure of the intracell and intercell components are same. Taking account of the thermal couplings in such a 2D network, two components respectively along the x and y directions can be decoupled from the imposed advections on each site to link the neighbors. When we further impose four equal-strength sources to one unit-structure, i.e., two hot and two cold sources respectively on corresponding diagonal sites, a diffusive analog to the quadrupole (Supplementary note) could be observed in the temperature field with a bulk quadrupole moment in the finite unit-structure, which further enables the dipole moments on the 1D edges and uncompensated charges 0D corners.

Due to the skew-Hermitian property obeyed by the thermal coupling matrix [27-30], the imposed advections act as the real hermiticities which are equivalent to the roles of gain and loss in photonics. While the heat exchanges induced by the intracell and intercell thermal processes provide the couplings between the neighboring sites. The opposite configurations of connections between two adjacent sites lead to the different orientations of isotherms in a target region

under the same advections (Supplementary Figure 2). Such an implementation further enables the effective positive and negative couplings in the thermal system. The wave-like solution on each site reveals the oscillatory propagation of the temperature fields. For simplification, we assign the effective negative couplings via inversely connecting the sites on the green coupling lines as shown in Figs. 1a and b. The thermal couplings between neighboring sites originate from both intracell and intercell heat exchanges. Solving the eigenvalue problem with the wave-like temperatures, the effective eigenvalues can be observed (Supplementary note).

The complex angular frequency and eigenvalues imply that both the advections and corresponding couplings result in the complex bands. The imaginary angular frequency originates from the intrinsic conduction and the heat exchanges, while the real angular frequency represents the effective momentum induced by the imposed advections towards different azimuths. These two parts simultaneously determine the amplitudes and the movements of the dynamic temperature field, thus retaining the possibilities of exciting the significant 1D edge and 0D corner states with two distinct recipes, i.e., the advective hermiticities and the coupling non-hermiticities. We then fabricate a square-lattice with 16 sites (Supplementary Figure) and immerse it into water.

We first focus on the HOTI motivated by modulating the advective hermiticity. The real phase diagrams of the first Brillouin zones under specific advections are presented in Supplementary note. When the imposed advective magnitudes are same and the directions are opposite, all the real bands degenerate indicating the gapless structure and the transition between nontrivial and trivial thermal states. When we slightly increase ω_{II} to maintain an advective difference, two gaps emerge between the first-second and the third-fourth bands, while the second and third bands are still degenerate. Further increasing ω_{II} , all the degeneracies lift and leave a complete open band structure. Such a transition from a gapless phase to a gapped phase via solely modulating the advective hermiticity is a class of topological quadrupole phase, thus implying the in-gap 0D and gapped 1D topological modes. We then calculate the dispersion relations to further validate the existences of these higher-order topological states. The robust in-gap corner state (red dots) and gapped edge state (blue dots) are

respectively presented in Figs. 1e and f. While the completely gapped bands illustrated in Fig. 1g depict a thermal analog of a trivial insulator.

We then fabricate a thermal system in a fluid ambient (Supplementary Figure) to demonstrate these nontrivial states. In order to ensure the topological transitions by solely modulating the advective hermiticity, the same structures are adopted to all coupling channels to remain the same intercell and intracell thermal exchange. Based on the calculated dispersion, one of the imposed advects on a pair of diagonal sites in one unit-structure is fixed at ω_I , while each advection ω_{II} on the other pair of diagonal sites can be flexibly modulated to seek the satisfied real-valued frequency. The eigenfrequency spectrum indicates that significant hierarchical features discretely distribute along the real-valued eigenfrequency and localize on one gapless imaginary-valued band (Supplementary Figure). When the real eigenfrequency respectively approaches limitations, the trivial bulk states showcase the gaps between these two branches in the real-valued band. We choose three sites respectively at the center, edge, and corner of the sample (marked as a square in Supplementary Figure), and capture their responses as plotted in Supplementary Figure. Here, we take the absolute values of the normalized temperatures to evaluate field intensities. Two peaks of the field intensities are observed at corresponding real eigenfrequency to the bulk branches. Similar to the responses in the bulk, the gapped edge states also exhibit two peaks as the gradient blue area. The four in-gap corner states emerge when further increasing ω_I . In that case, only one peak is found on the field intensity distribution. To further experimentally demonstrate these higher-order states, we measure the temperature distributions by modulating the advects as shown in Figs. 2a ~ c. When adjusting ω_{II} to the corresponding peaks of edge and corner states, the temperature amplitudes and field intensities would be larger at the corner and edge as illustrated in Figs. 2d and e. Further selecting the advects at bulk state, the temperature intensities in the central domain are much higher than the ones at the corners and edges (Fig. 2f). These theoretical and experimental findings reveal the higher-order topological states in real-valued bands solely induced and modulated by the advective hermiticities in a thermal system.

As implied in the eigenvalues (Supplementary Equation 10), such higher-order topological states can be also motivated by the inherent non-hermiticities and captured along the imaginary-valued bands. Note that, such states in these imaginary-valued bands can be theoretically observed either in a skew-Hermitian thermal system without advections ($\omega_I = \omega_{II} = 0$) or a non-Hermitian heat transfer with advections possessing the same magnitudes and direction ($\omega_I = \omega_{II} \neq 0$). Here, we focus on the non-Hermitian strategy and further demonstrate the higher-order states under a pair of small magnitude advections. In that case, the real-valued band is gapless that can be adopted to distinguish the states along the gapped imaginary-valued band (Supplementary Note 4). The intracell and intercell thermal coupling strengths should be also different at this stage. The coupling strengths can be manipulated by the heat exchanges within the intercell and intracell channels. For simplification, we keep the same intercell couplings as the case shown in Fig. 1. We further modify the structure by enlarging the intracell coupling channels (Fig. 3a). Such implementations enable the modulations of β ranging from 0 to 1. The imaginary phase diagrams of the first Brillouin zones of one modified square-lattice are presented in Supplementary note. Similar to the modulations with advective hermiticities, all the imaginary-valued bands degenerate with the same intracell and intercell couplings ($\beta = 1$). While two gaps between the 1st-2nd and 3rd-4th bands are observed by modulating β , thus revealing the 1D edge and 0D corner states in the imaginary-valued bands. The dispersion relations further validate the existences of in-gap corner (Fig. 3b), gapped edge (Fig. 3c), and trivial bulk (Fig. 3d) states along the imaginary eigenfrequencies at tailored β .

Then, we construct the thermal system with the modified square-lattices as illustrated in Supplementary Figure. When β respectively approaches near-zero and 1 in the experiments, two branches are localized along imaginary band and imply the trivial bulk states (Supplementary Figure). When selecting β in the range of 0 to 1, two gapped edge and one in-gap corner states are also expected. The field intensities on imaginary-valued bands further verify the above hypothesis with two peaks on the central/edge and one peak on the corner of the measured sites (Supplementary Figure 4a). Such features overlap well with the experimental temperature field distributions (Figs. 4a ~ c) and the measured intensity profiles (Figs.

4d ~ f) under corresponding β . These results (Figs. 2 and 4) demonstrate the proof-of-concept higher-order features in non-Hermitian thermal systems via modulating either the imposed advections (hermiticity) or the thermal coupling strengths (non-hermiticity).

This work reports on the construction of an effective quadrupole moment in thermal diffusion and observes the non-Hermitian thermal HOTIs for the first time. Our results highlight the fundamental differences of these higher-order features that radically depart from the widespread wisdom that occurs only on the real-valued band in wave fields. The complex eigenvalues enable the phase transitions both on the real- and imaginary-valued bands. By modulating either the advective hermiticity or the thermal coupling non-hermiticity, the experimental demonstrations exhibit significant hierarchies of topological states in the temperature fields. We envision an entirely new territory of HOTI in diffusive context that may reveal exotic physics on complex bands. This work also facilitates the manipulation of diffusive fields using these bulk, edge, and corner states.

References

1. Xiao, M., Ma, G., Yang, Z., Sheng, P., Zhang Z., Chan, C. T. Geometric phase and band inversion in periodic acoustic systems. *Nat. Phys.* **11**, 240-244. (2015).
2. Yan, Q., Liu, R., Yan, Z., Liu, B., Chen, H., Wang, Z., Lu, L. Experimental discovery of nodal chains. *Nat. Phys.* **14**, 461-464 (2018).
3. Yang, Y., Gao, Z., Xue, H., Zhang, L., He, M., Yang, Z., Singh, R., Chong, Y., Zhang, B., Chen, H. Realization of a three-dimensional photonic topological insulator. *Nature* **565**, 622–626 (2019).
4. Patil, V. P., Sandt, J. D., Kolle, M., Dunkel, J. Topological mechanics of knots and tangles. *Science* **367**, 71-75 (2020).
5. Chen, Z., Segev, M. Highlighting photonics: looking into the next decade. *elight* **1**, 2 (2021).
6. Hasan, M. Z., Kane, C. L. Colloquium: topological insulators. *Rev. Mod. Phys.* **82**, 3045 (2010).

7. Bansil, A., Lin, H., Das, T. Colloquium: topological band theory. *Rev. Mod. Phys.* **88**, 021004 (2016).
8. Chiu, C. K., Teo, J. C. Y., Schnyder, A. P., Ryu, S. Classification of topological quantum matter with symmetries. *Rev. Mod. Phys.* **88**, 035005 (2016).
9. Rudner, M. S., Lindner, N. H., Berg, E., Levin, M. Anomalous edge states and the bulk-edge correspondence for periodically driven two-dimensional systems. *Phys. Rev. X* **3**, 031005 (2013).
10. Feng, L., Wong, Z. J., Ma, R. M., Wang, Y., Zhang, X. Single-mode laser by parity-time symmetry breaking. *Science* **346**, 972 (2014).
11. Feng, L., El-Ganainy, R., Ge, L. Non-Hermitian photonics based on parity-time symmetry. *Nat. Photonics* **11**, 752-762 (2017).
12. Assawaworrarit, S., Yu, X., Fan, S. Robust wireless power transfer using a nonlinear parity-time-symmetric circuit. *Nature* **546**, 387-390 (2017).
13. Cerjan, A., Huang, S., Wang, M., Chen, K. P., Chong, Y., Rechtsman, M. C. Experimental realization of a Weyl exceptional ring. *Nat. Photonics* **13**, 623-628 (2019).
14. Liu, T., He, J. J., Yang, Z., Nori, F. Higher-order Weyl-exceptional-ring semimetals. *Phys. Rev. Lett.* **127**, 196801 (2021).
15. Weidemann, S., Kremer, M., Helbig, T., Hofmann, T., Stegmaier, A., Greiter, M., Thomale, R., Szameit, A. Topological funneling of light. *Science* **368**, 311-314 (2020).
16. Li, L., Lee, C. H., Gong, J. Topological switch for non-Hermitian skin effect in cold-atom systems with loss. *Phys. Rev. Lett.* **124**, 250402 (2020).
17. Benalcazar, W. A., Bernevig, B. A., Hughes, T. L. Quantized electric multipole insulators. *Science* **357**, 61-66 (2017).
18. Serra-Garcia, M., Peri, V., Süsstrunk, R., Bilal, O. R., Larsen, T., Villanueva, L. G., Huber, S. D.. Observation of a phononic quadrupole topological insulator. *Nature* **555**, 342-345 (2018).

19. Peterson, C. W., Benalcazar, W., A., Hughes, T. L., Bahl, G. A quantized microwave quadrupole insulator with topologically protected corner states. *Nature* **555**, 346-350 (2018).
20. Fan, H., Xia, B., Tong, L., Zheng, S., Yu, D. Elastic higher-order topological insulator with topologically protected corner states. *Phys. Rev. Lett.* **122**, 204301 (2019).
21. Peterson, C. W., Li, T., Benalcazar, W. A., Hughes, T., Bahl, G. A fractional corner anomaly reveals higher-order topology. *Science* **368**, 1114-1118 (2020).
22. Luo, L., Wang, H., Lin, Z., Jiang, B., Wu, W., Li, F., Jiang, J.-H. Observation of a phononic higher-order Weyl semimetal. *Nat. Mater.* **20**, 794-799 (2021).
23. Luo, X. W., Zhang, C. Higher-order topological corner states induced by gain and loss. *Phys. Rev. Lett.* **123**, 073601, (2019).
24. Qi, Y., Qiu, C., Xiao, M., He, H., Ke, M., Liu, Z. Acoustic realization of quadrupole topological insulators. *Phys. Rev. Lett.* **124**, 206601, (2020).
25. Gao, H., Xue, H., Gu, Z., Liu, T., Zhu, J., Zhang, B. Non-Hermitian route to higher-order topology in an acoustic crystal. *Nat. Commun.* **12**, 1888 (2021).
26. Zhang, X., Tian, Y., Jiang, J.-H., Lu, M., Chen, Y. Observation of higher-order non-Hermitian skin effect. *Nat. Commun.* **12**, 5377 (2021).
27. Li, Y., Peng, Y. G., Han, L., Miri, M. A., Li, W., Xiao, M., Zhu, X. F., Zhao, J., Alù, A., Fan, S., Qiu, C.-W. Anti-parity-time symmetry in diffusive systems. *Science* **364**, 170–173 (2019)
28. Xu, G., Li, Y., Li, W., Fan, S., Qiu, C.-W. Configurable phase transitions in topological thermal material. *Phys. Rev. Lett.* **127**, 105901 (2021).
29. Xu, G., Yang, Y., Zhou, X. Chen, H., Alu, A., Qiu, C.-W. Diffusive topological transport in spatiotemporal thermal lattices. *Nat. Phys.* **18**, 450-456 (2022).

30. Xu, G., Li, W., Zhou, X., Li, H., Li, Y., Fan, S., Zhang, S., Christodoulides, D. N., Qiu, C.-W. Observation of Weyl exceptional rings in thermal diffusion. *Proc. Natl. Acad. Sci. U.S.A.* **119** (15) e2110018119
31. Fan, C. Z., Gao, Y., Huang, J. P. Shaped graded materials with an apparent negative thermal conductivity. *Appl. Phys. Lett.* **92**, 251907 (2008).
32. Li, Y., Li, W., Han, T., Zheng, X., Li, J., Li, B., Fan, S., Qiu, C.-W. Transforming heat transfer with thermal metamaterials and devices. *Nat. Rev. Mater.* **6**, 488-507 (2021).
33. Xu, G., Dong, K., Li, Y., Li, H., Liu, K., Li, L., Wu, J., Qiu, C.-W. Tunable analog thermal material. *Nat. Commun.* **11**, 1-9 (2020).
34. Guo, J., Xu, G., Tian, D., Qu, Z., Qiu, C.-W. Passive ultra-conductive thermal metamaterials. *Adv. Mater.* 2200329 (2022).
35. Xu, L., Xu, G., Huang, J., Qiu, C.-W. Diffusive Fizeau drag in spatiotemporal thermal metamaterials. *Phys. Rev. Lett.* **128**, 145901 (2022).

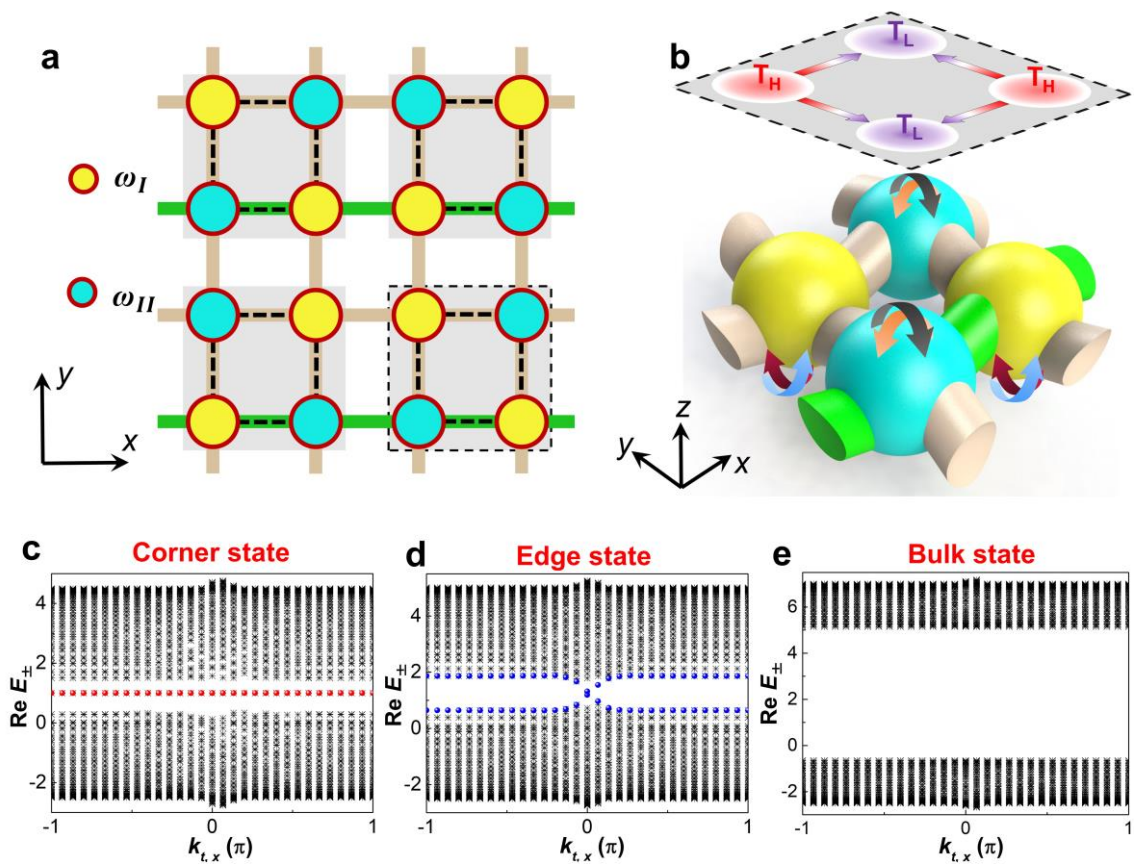


Fig. 1. Higher-order topological insulator induced by advective hermiticities in thermal diffusion and phase diagrams.

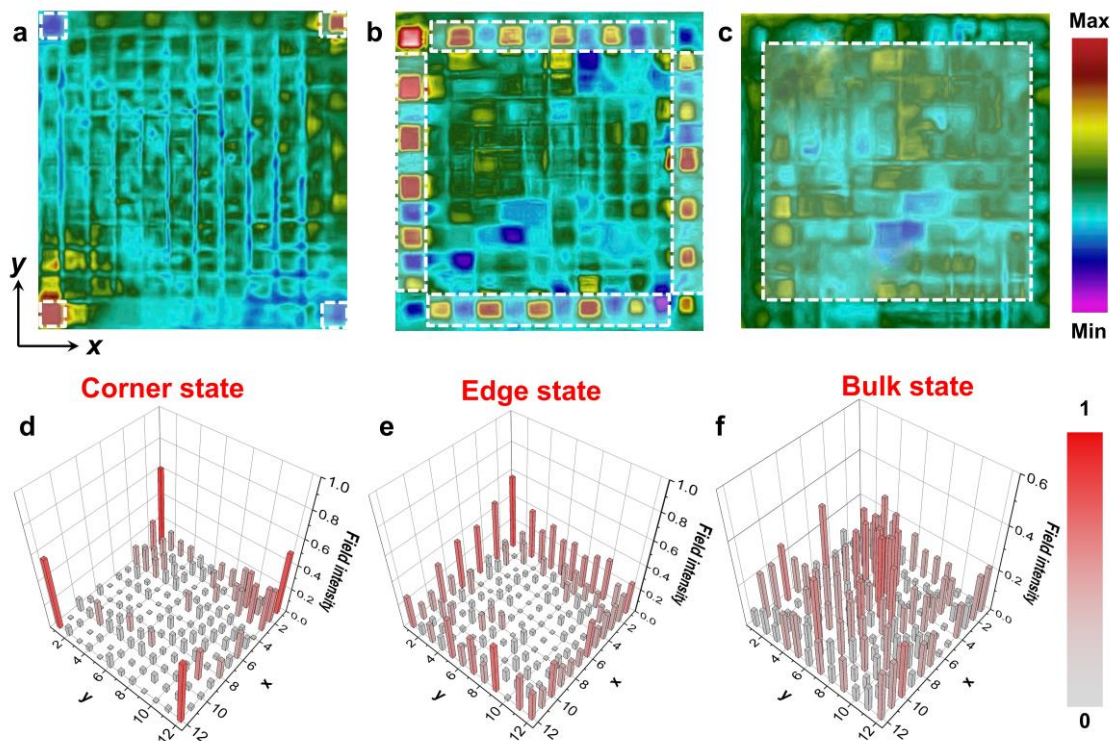


Fig. 2. Experimental observations of the higher-order topological states in thermal diffusion solely induced by advective hermiticities.

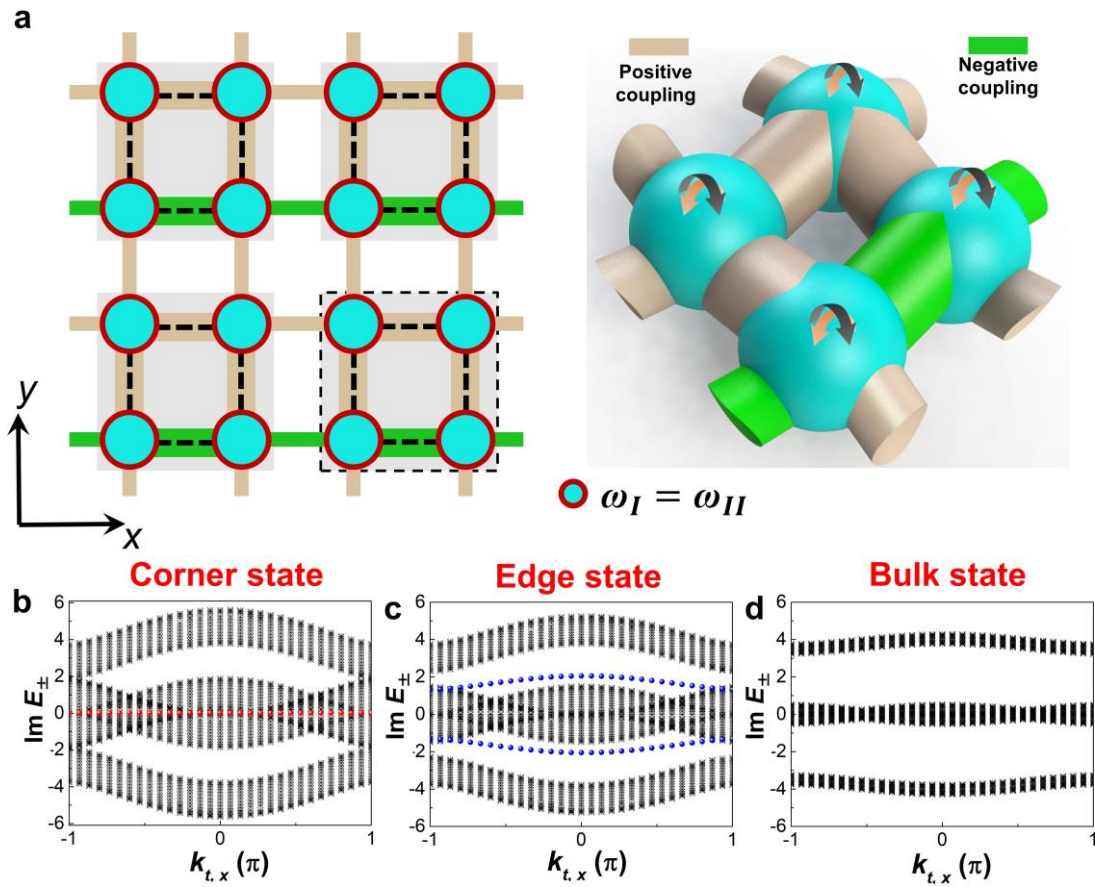


Fig. 3. Higher-order topological insulator induced by coupling non-hermiticities in thermal diffusion and phase diagrams.

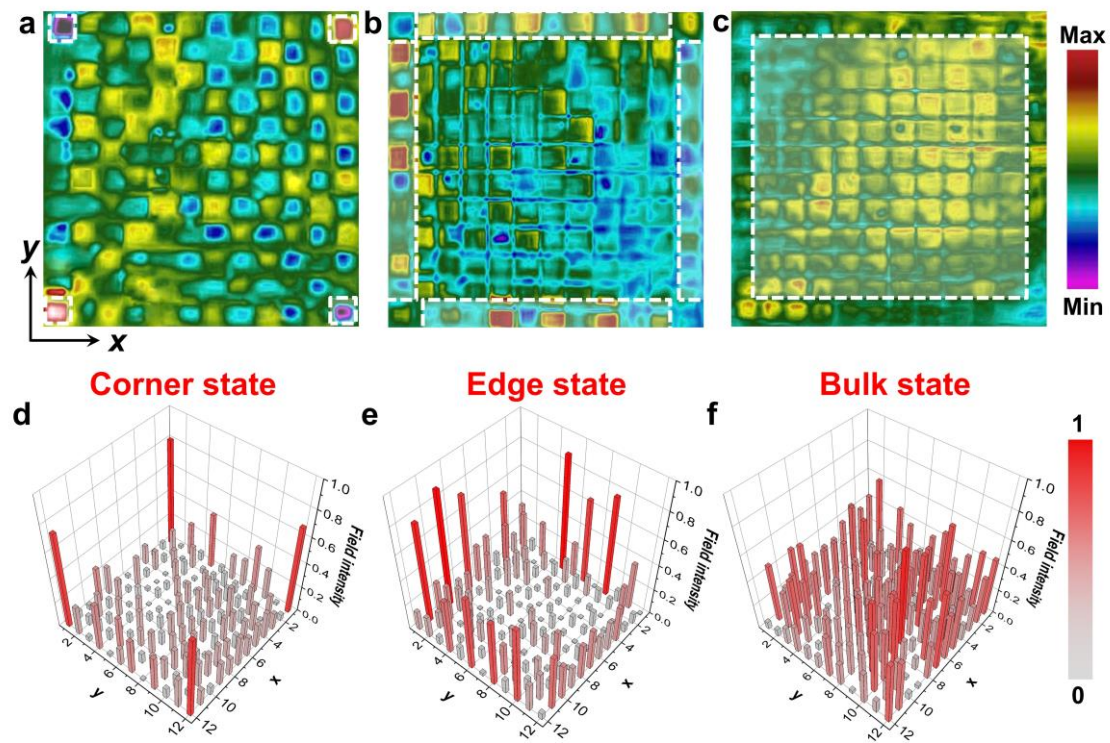


Fig. 4. Experimental observations of the higher-order topological states in thermal diffusion solely induced by coupling non-hermiticities.